JOURNAL OF PROPULSION AND POWER
Vol. 10, No. 6, Nov.–Dec. 1994

OH Laser-Induced Fluorescence Velocimetry Technique for Steady, High-Speed, Reacting Flows

Kurt G. Klavuhn,* Gautam Gauba,* and James C. McDaniel†
University of Virginia, Charlottesville, Virginia 22903

A high-resolution OH laser-induced fluorescence velocity measurement technique was developed for use in steady, high-speed, reacting flows. A narrow-linewidth laser source was tuned through an isolated OH absorption line to measure the Doppler-shifted line center frequency relative to an iodine reference line. A counterpropagating-beam approach was used to eliminate the collisional impact shift and minimize systematic errors. Results from pointwise measurements of velocity in a unique reacting underexpanded jet facility are compared to an axisymmetric Navier-Stokes calculation with finite-rate chemical kinetics as a test of the technique over a wide range of flow conditions. The measured and calculated velocities in the supersonic jet core agree on average to within 1.3%. The uncertainty in the velocity measurement in the jet core was on average ±6.0% for a single measurement and ±3.5% for the average value of three scans. Potential errors caused by absorption effects were not detected in these measurements.

Introduction

OVER the past decade, renewed interest in air-breathing hypersonic vehicles has spawned major research and development programs in the field of hypersonic propulsion. The focus of the effort at high speeds is the development of the supersonic-combustion-ramjet (scramjet). Development of this type of engine presents a unique challenge because ground test facilities are not able to reproduce the Mach number and thermodynamic conditions of the entire scramjet flight envelope. Propulsion engineers must, therefore, rely on computational fluid dynamics (CFD) models to aid with the design optimization and performance prediction for those conditions not obtainable with current test facility technology. Before CFD models can be successfully applied, however, confidence in their predictive abilities must be established through comparison with experimental data. The objective of the work reported herein is to develop a spatially resolved velocity measurement technique in steady, high-speed, reacting flows to enable the collection of data with sufficient accuracy for CFD validation.

Measurement in a supersonic combustion flowfield requires a nonintrusive optical technique since mechanical probes can alter the fluid dynamics and the chemical kinetics. Various laser-based spectroscopic techniques have been developed for providing accurate quantitative flowfield properties with excellent spatial resolution.[1] In spite of all the recent advancements in optical diagnostics, however, there is still a serious need for an accurate velocity measurement technique for high-speed reacting flows.

Particle-based Mie scattering techniques, such as laser-Doppler velocimetry (LDV) and particle image velocimetry (PIV), have proven to be highly successful, nonintrusive diagnostic tools for a variety of incompressible and low-speed compressible flows. However, in high-speed compressible flows with large velocity gradients, particle-based techniques suffer from particle lag and centrifugal effects due to the large inertia of the seed particles relative to that of the gas molecules.[2] Methods to correct for the particle velocity bias have been reported,[3] but these methods require full flowfield solutions and knowledge of the particle size distribution, which are usually not available.

Time-of-flight approaches, such as the RELIEF[4] method, where a line of oxygen molecules is tagged via stimulated Raman scattering and later interrogated via laser-induced fluorescence, or the OH-flow-tagging[5] method, where a KrF excimer laser generates a zone of enhanced OH concentration via the photolysis of water molecules and later interrogates the generated OH via laser-induced fluorescence using a second UV laser, have been successfully used to measure velocity in low- and high-speed flows. However, these techniques are relatively complex and do not have the spatial accuracy inherent in single-point techniques.

Doppler-shift methods measure the frequency shift of elastic or inelastic scattering from atoms or molecules in the flow, and have evolved as the most promising spatially-resolved velocity measurement technique for high-speed compressible flows. Miles and Lempert[6] have demonstrated a technique for qualitative and quantitative velocity field imaging using filtered Rayleigh scattering. Their technique provides density field images for molecules with velocities in a range determined by an iodine vapor filter used to selectively separate Doppler-shifted Rayleigh-scattered light from the unshifted background light. Since Rayleigh scattering cross sections are typically very small, the measurement accuracy in flows with strong background signals is limited.

Coherent scattering techniques for measuring molecular velocity have been proposed using coherent Raman spectroscopy,[7] coherent antistokes Raman spectroscopy,[8] stimulated Raman gain spectroscopy,[9] inverse Raman spectroscopy,[10,11] and stimulated Rayleigh-Brillouin-gain spectroscopy.[12] Since N_2 can be used as the scatterer, these Raman techniques, as well as the Rayleigh technique mentioned above, are of particular interest because of their direct applicability to unseeded wind-tunnel flows. Although most of these techniques have been successfully demonstrated in supersonic flows, they have not been widely used because of their complexity and relatively low signal strength.

Laser-induced fluorescence (LIF) has proven to be the most useful of the Doppler-shift methods due to its relatively large

Presented as Paper 92-3422 at the AIAA/SAE/ASME/ASEE 28th Joint Propulsion Conference and Exhibit, Nashville, TN, July 6–8, 1992; received July 17, 1992; revision received Jan. 26, 1994; accepted for publication April 29, 1994.

*Graduate Research Assistant, Aerospace Research Laboratory, Department of Mechanical, Aerospace, and Nuclear Engineering. Student Member AIAA.

†Associate Professor, Aerospace Research Laboratory, Department of Mechanical, Aerospace, and Nuclear Engineering. Member AIAA.

signal strength and its ability to discriminate the spectrally shifted signal from elastic beam scatter. Laser-induced iodine fluorescence (LIIF) has been used extensively as a diagnostic tool for nonreacting compressible flows. The LIIF technique uses iodine as the absorption species seeded into the flow. Quantitative velocity measurements using LIIF[13,14] and planar LIIF[15,16] have been reported for a variety of nonreacting flows. Similar techniques using LIF of Na seeded in N_2,[17] Na seeded in He,[18] and NO seeded in air[19,20] have also been demonstrated. However, the addition of seed molecules into chemically reacting flows is usually not an option due to the chemical interactions between the seed material and the flow; therefore, a naturally occurring specie must be used. Marinelli et al.[21] took advantage of the presence of Cu atoms seeded in the flow during sputtering of the electrodes in a high-enthalpy arcjet thruster for velocity measurements using LIF of Cu. Erwin et al.[22] used LIF of nascent H atoms for velocity measurements in an ammonia-propelled arcjet thruster, and Liebeskind et al.[23] used LIF of H atoms from the dissociation of H_2 for velocity measurements in a hydrogen arcjet.

In the types of supersonic hydrogen-air combustors considered here, the OH molecule is an abundant intermediate flame species, and its (1,0) and (0,0) absorption bands of the $A^2\Sigma^+$-$X^2\Pi$ system in the 280–320-nm range are easily accessible with available uv laser sources. Quantitative pointwise OH LIF velocity measurements in a methane-air freejet using a rapid tuning, narrow-band, continuous-wave (CW) dye laser[24] have been reported; however, frequency-doubled CW lasers do not provide enough power to extend the single-point technique to planar measurements. Paul and Hanson[25] used a pulsed broadband XeCl excimer laser for planar velocity measurements in a hydrogen-air freejet. Although the broadband technique shows promise for measuring velocity with both spatial and temporal resolution, it relies on accurate characterization of the laser line shape, is sensitive to any flowfield variable that changes the absorber line shape, and is limited as to the maximum range of measurable Doppler shifts.

The development of an accurate, spatially resolved OH LIF velocity measurement technique for application in steady, supersonic, reacting flows is presented in this article. Pointwise measurements of velocity in a reacting underexpanded jet facility were made to examine the accuracy of the technique over a broad range of flow conditions. This technique is being developed for planar velocity measurements in a model supersonic combustion ramjet flowfield and, together with other measurements in this flowfield, will provide a complete set of data for CFD validation.

OH LIF Velocity Measurement

The approach for measuring velocity in high-speed reacting flows is based on detection of the laser-induced fluorescence from a Doppler-shifted OH absorption line. For this technique, a narrow-linewidth laser source is tuned through an isolated portion of the OH absorption spectrum, and the resulting fluorescence is collected normal to the laser beam. The velocity of the gas molecules causes them to absorb at a frequency that is Doppler-shifted from the static line center frequency by

$$\Delta\nu_d = \frac{1}{2\pi}(\boldsymbol{k}\cdot\boldsymbol{u}) \tag{1}$$

where $\Delta\nu_d$ is the Doppler shift, $\boldsymbol{k}$ is the light propagation vector with magnitude $|\boldsymbol{k}| = 2\pi/\lambda$, and $\boldsymbol{u}$ is the gas velocity vector. A complication arises due to an additional frequency shift, termed collisional impact shift, caused by elastic collisions between the emitting molecules and the surrounding gas.[26] The impact shift depends on the local thermodynamic conditions that can vary greatly in a high-speed reacting flow. Figure 1 illustrates an approach for canceling the impact shift

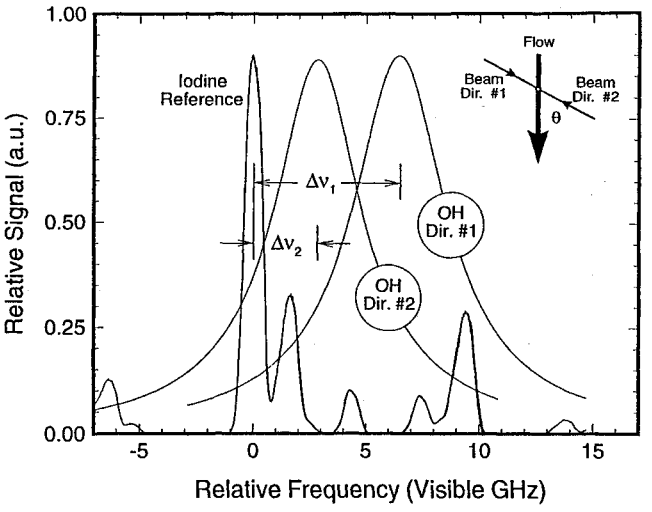

Fig. 1 OH LIF velocity measurement technique using counterpropagating beams to eliminate the collisional impact shift.

effects.[27] This approach uses counterpropagating laser beams, such that for each point in the flow the OH absorption is Doppler-shifted in an opposite sense for direction no. 1 than for direction no. 2, (i.e., $\Delta\nu_{d1} = -\Delta\nu_{d2} = \Delta\nu_d$). The impact shift, $\Delta\nu_I$, is the same for the two laser beam directions, so that $\Delta\nu_1 = \Delta\nu_{d1} + \Delta\nu_I$, and $\Delta\nu_2 = \Delta\nu_{d2} + \Delta\nu_I$, where the total line-center shifts $\Delta\nu_1$ and $\Delta\nu_2$ are measured relative to an absolute frequency reference, an iodine absorption line in this case. The Doppler shift is given by one-half the difference between the two total shifts

$$\Delta\nu_d = \frac{\Delta\nu_1 - \Delta\nu_2}{2} = \frac{(\Delta\nu_{d1} + \Delta\nu_I) - (\Delta\nu_{d2} + \Delta\nu_I)}{2}$$
$$= \frac{\Delta\nu_{d1} - \Delta\nu_{d2}}{2} = \frac{\Delta\nu_d - (-\Delta\nu_d)}{2} \tag{2}$$

and the impact shift is thereby removed. Other advantages to using counterpropagating beams in removing systematic errors in the measurement will be discussed later.

OH LIF

A model of the OH LIF strategy employed in this work is described below, with particular emphasis on optimizing this strategy for quantitative velocity measurements. The model is later used to calculate the expected signal-to-noise ratio (SNR) for a test flowfield since, as will be later shown, the measurement uncertainty is directly proportional to SNR^{-1}. Since the model does not include a detailed analysis of the various energy transfer mechanisms, it is intended for signal level estimation purposes only.

For a given excitation and detection system, the fluorescence signal is dependent on the choice of the absorption line and on the local thermodynamic conditions of the flow at the measurement location. The chosen absorption line should be relatively isolated (i.e., free from interference from adjacent lines), have a sufficiently large absorption coefficient, represent a significant fraction of the total Boltzmann population, and be sufficiently spectrally separated from the emitting band to allow efficient discrimination of the fluorescence emission from elastically scattered laser radiation (e.g., Mie or Rayleigh scattering). The Q-branch of the (1,0) band of OH offers relatively large absorption coefficients[28] and is separated from the strongly radiating (1,1) and (0,0) bands by ~25 nm.[29] Figure 2 illustrates a model of the important coupling processes between the $X^2\Pi$ ground electronic state and the $A^2\Sigma^+$ excited electronic state for (1,0) excitation. For this particular

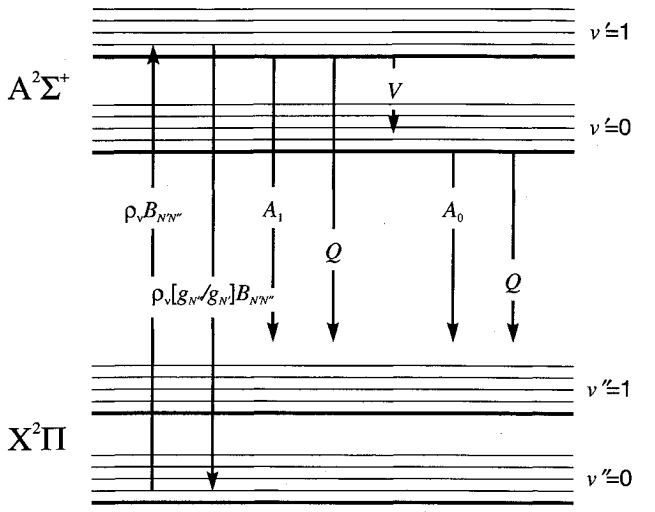

Fig. 2 Important rate processes for OH (1,0) excitation with (1,1) and (0,0) band detection.

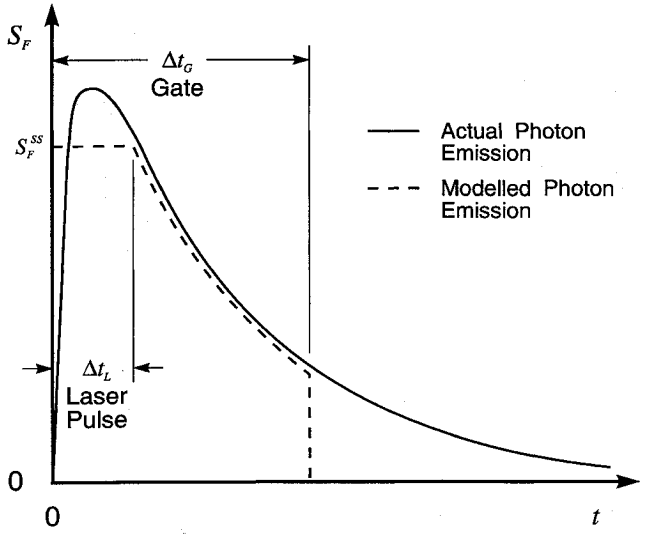

Fig. 3 Gated fluorescence detection when the fluorescence lifetime exceeds the laser pulse duration.

model, the energy transfer among the individual rotational levels in each vibrational level is not considered in detail and, therefore, is not shown. The incident laser beam is tuned to an electronic resonance, thereby inducing transitions $\rho_\nu B_{N'N''}$ from an isolated rotational level in the $\nu'' = 0$ ground electronic state to an isolated rotational level in the $\nu' = 1$ excited electronic state. Since the excited molecules are not in thermal equilibrium, they will decay back to the ground state via spontaneous emission A_1, stimulated emission $\rho_\nu[g_{N''}/g_{N'}]B_{N'N''}$, or collisional quenching Q from $\nu' = 1$, or via collisional transfer V to $\nu' = 0$, followed by spontaneous emission A_0 and collisional quenching Q from $\nu' = 0$.

When using LIF to make quantitative velocity measurements, it is often necessary to gate the fluorescence signal to minimize the detection of background radiation and to avoid motional blurring. The issue of motional blurring becomes particularly important when making planar measurements in fast, low-pressure flows where the fluorescence lifetime is often longer than the time it takes for an emitting specie to travel between pixels in the imaging plane. Conversely, in order to maximize the number of photons collected, one would like to use as large a gate as possible. Since the fluorescence lifetime in low-pressure gaseous flows can significantly exceed the laser temporal width, it is important to model the temporal history of the fluorescence to account for gate times longer than the laser pulse. The present temporal model, shown in Fig. 3, accounts for this by assuming that the total number of photons collected S_F^{tot}, includes those emitted at a steady-state rate during the laser pulse, plus those emitted after the laser pulse at an exponentially-decreasing rate until the end of the gate period.

Using the simple four-level model shown in Fig. 2, and including both the steady-state and exponentially decaying solutions as illustrated in Fig. 3, the total fluorescence signal S_F^{tot} (no. of photons), can be expressed as[30]

$$S_F^{tot} = \eta(\Omega/4\pi)V_C N_{SS}(S_1^{SS} + S_0^{SS} + S_1^{ED} + S_0^{ED}) \quad (3)$$

where the numbered subscripts refer to the emitting vibrational levels. The steady-state terms are given by

$$S_1^{SS} = A_{11}^{eff}\Delta t_L \quad (4)$$

$$S_0^{SS} = A_{00}^{eff}\tau_0 V\Delta t_L \quad (5)$$

and the exponentially decaying terms are given by

$$S_1^{ED} = A_{11}^{eff}\tau_1\{1 - \exp[(\Delta t_L - \Delta t_G)/\tau_1]\} \quad (6)$$

$$S_0^{ED} = A_{00}^{eff}\tau_0\tau_1 V\big(\tau_1\{1 - \exp[(\Delta t_L - \Delta t_G)/\tau_1]\}/(\tau_1 - \tau_0) + \tau_0^2\{1 - \exp[(\Delta t_L - \Delta t_G)/\tau_0]\}/\tau_1(\tau_1 - \tau_0)\big) \quad (7)$$

for narrow-linewidth excitation and filtered detection of the spectrally overlapping (1,1) and (0,0) band fluorescence. In Eqs. (3–7), η is the detector quantum efficiency, Ω is the collection solid angle (ster), V_C is the collection volume (m^3), N_{SS} is the steady-state number density of the directly pumped energy level (m^{-3}), Δt_L is the laser pulse duration (s), Δt_G is the gate width (s), A_{11}^{eff} and A_{00}^{eff} are the effective photon emission rates (s^{-1}) for the (1,1) and (0,0) bands, respectively, and V is the vibrational transfer rate (s^{-1}) from $\nu' = 1$ to $\nu' = 0$. τ_1 and τ_0 are the total lifetimes of $\nu' = 1$ and $\nu' = 0$, which are defined by $\tau_1 = 1/(A_1 + Q + V)$ and $\tau_0 = 1/(A_0 + Q)$, where A_1 and A_0 are the total Einstein coefficients for spontaneous emission (s^{-1}) from $\nu' = 1$ and $\nu' = 0$, respectively, and Q is the collisional quenching rate (s^{-1}). The details of the calculation of the total fluorescence signal using Eqs. (3–7) are given in the Appendix.

Reacting Underexpanded Jet Experiment

Reacting Underexpanded Jet

The OH LIF velocity measurement technique was calibrated using a unique reacting underexpanded jet facility.[31] The jet facility, illustrated in Fig. 4, consists of a small ceramic-lined combustion chamber that contains a stoichiometric hydrogen-air flame, the products of which are accelerated through a 3.15-mm-i.d. alumina tube into a low-pressure chamber to form a reacting underexpanded jet. Alumina was used to provide a high-temperature boundary to minimize quenching of the OH. Figure 5 outlines the main features of the jet flowfield. The high-pressure gas leaving the exit of the tube undergoes rapid expansion into the low pressure of the surrounding chamber. The resulting expansion waves reflect off the constant pressure boundary as compression waves and coalesce to form the characteristic barrel shock structure that terminates with a Mach disk.

The flowfield properties for a stoichiometric hydrogen-air jet with a source temperature $T_0 = 2000$ K, a source pressure $P_0 = 160$ kPa (1.58 atm), and a chamber pressure $P_b = 11$ kPa (0.11 atm), were calculated using an axisymmetric version of SPARK, a Reynolds-averaged Navier-Stokes code with finite-rate chemistry that uses a 9-species (H_2, O_2, H_2O, OH, H, O, HO_2, H_2O_2, and inert N_2), 18-reaction chemistry model.[32] The conditions in the combustion chamber were determined using an equilibrium code.[33] The conditions through the ceramic tube were calculated assuming one-dimensional adi-

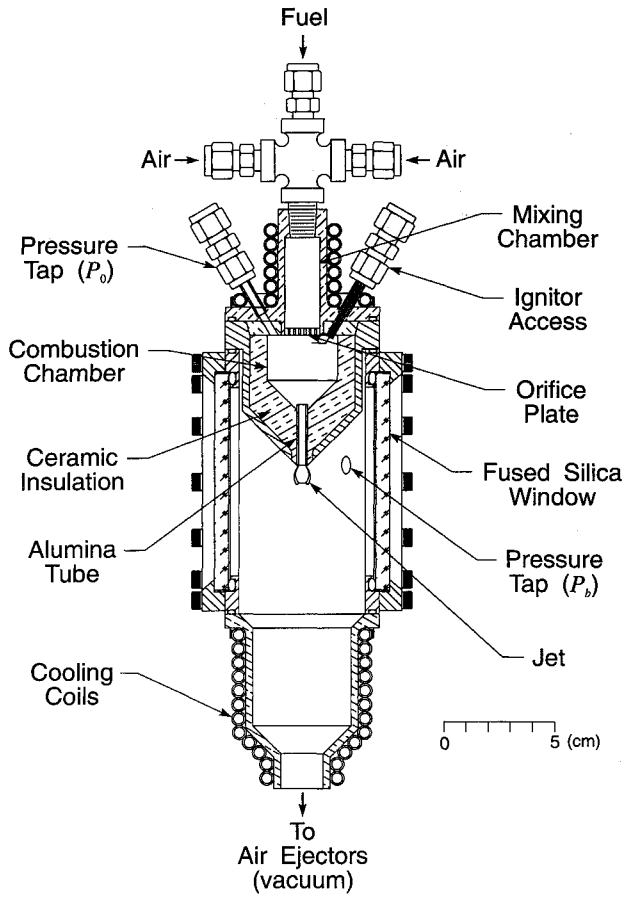

Fig. 4 Reacting underexpanded jet facility.

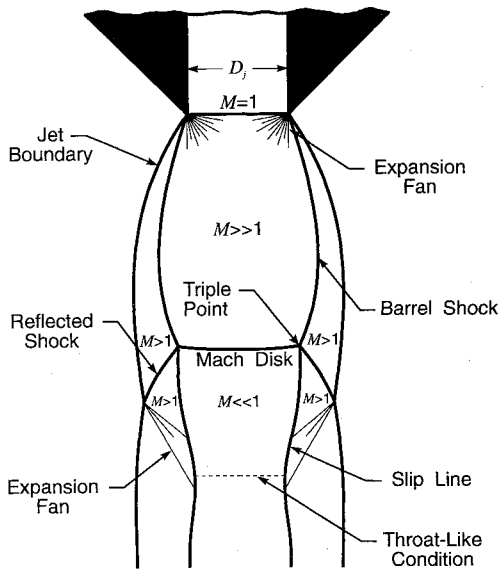

Fig. 5 Flowfield schematic for the reacting underexpanded jet.

abatic flow with friction (Fanno line) and frozen chemistry. The flow properties at the tube exit were used as the inflow boundary conditions for the axisymmetric calculation. Figure 6 shows calculated contours of Mach number and temperature, and Fig. 7 shows contours of pressure and OH number density. Centerline values are plotted independently to better illustrate the wide range of thermodynamic conditions that is representative of supersonic reacting flows and freejet expansions.

Laser System

Figure 8 is a schematic of the optical setup for the reacting underexpanded jet experiment, including the narrow-linewidth laser source required for the OH LIF velocity measurements. An argon ion laser (Spectra Physics 2030) pumps a CW ring dye laser (Spectra Physics 380A) with 4 W at 514.4 nm to produce a 500-mW tunable CW beam at 566 nm with a measured linewidth of ~20 MHz-VIS (VIS denotes "in the visible"). Rhodamine 560 perchlorate is used in the ring laser because of its high gain at the wavelength of interest. The output of the ring laser is passed through a frequency stabilizer (Spectra Physics 388) for active stabilization, a necessity in noisy environments when scan times are on the order of minutes. A fraction (5%) of the throughput from the frequency stabilizer is split, and a portion is sent to a 10-GHz-VIS spectrum analyzer (Spectra Physics 450-04) to monitor laser stability, while the remainder is chopped and sent to an iodine static cell and to a 2-GHz-VIS confocal interferometer (Spectra Physics 450-03) for phase-sensitive detection of absolute and relative frequency, respectively. An additional beam sample is sent to a wavemeter (Burleigh Wavemeter Jr.) for wavelength measurement. The remainder of the dye laser beam is amplified with a pulsed dye amplifier (Spectra Physics PDA-1), pumped by a Nd:YAG laser (Spectra Physics DCR-3). A $4.90(10)^{-5}$ solution of Rhodamine 590 in methanol is used in the first amplifier stage and a $3.21(10)^{-5}$ molar solution is used in the remaining two stages to produce 15-mJ, 13-ns pulses at 566 nm, with a measured, nearly transform-limited linewidth of ~110 MHz-VIS, and less than 1% amplified stimulated emission (ASE). Unpreventable ASE (i.e., ASE that is not suppressed by the spatial filters and slightly tilted optics in the pulsed dye amplifier) is blocked by an optical isolator on the input side of the amplifier to prevent feedback from destabilizing the ring laser. The pulse-amplified beam is frequency doubled in a wavelength extender (Spectra Physics WEX-1), resulting in 0.3-mJ pulses at 283 nm with an estimated linewidth of ~155 MHz-uv (uv denotes "in the ultraviolet"), which is less than 2% of typical OH linewidths in high-speed flames.

Procedure

The 5-mm-diam uv beam is focused with a $f = 340$ mm lens on the jet centerline at an angle of 54 deg to the direction of the flow. Fluorescence is detected by a photomultiplier tube (RCA 4837) through $f/1.9$ optics oriented at right angles to the laser beam. A combination bandpass and cuton filter (1-mm-thick Schott UG-11 and 4-mm-thick Schott WG-305) is used to discriminate the (0,0) and (1,1) band fluorescence from elastic beam scatter. The photomultiplier tube is set to a bias of −610 V. When making measurements in the high-density regions of the flow, a 0.7-ND filter is added to keep the signal level within the linear range of the photomultiplier tube. The intersection of the focused beam (waist diam = 150 μm) and the collection solid angle (aperture diam = 150 μm) provides a measurement volume of $\sim 2.7(10)^{-3}$ mm^3. The reacting underexpanded jet facility is mounted on translation stages to allow complete access to the entire jet flowfield without moving the optics. In addition, one mirror is mounted on a precision translation stage so that the beam can be directed through the jet in either counterpropagating direction by moving the mirror in and out of the beam path. Laser scanning and data acquisition are fully automated and controlled by a laboratory PC. The laser is scanned through a 60-GHz-uv (30-GHz-VIS) region centered on the (1,0) $Q_1(5)$ absorption line. The OH fluorescence and laser power signals are amplified with 300-MHz amplifiers (SRS SR445). The amplified signals are gated at 40 ns (chosen as a compromise between signal level and motional blurring in future planar imaging applications), and averaged over 10 laser pulses with gated integrators (SRS SR250), and routed, along with the iodine static cell and interferometer signals, to the computer for storage. A total of 1500 data points (i.e., one data point every 20-MHz-VIS increment tuned by the laser) are collected for the iodine and interferometer signals in order to resolve the narrow spectral features; however, the much broader OH

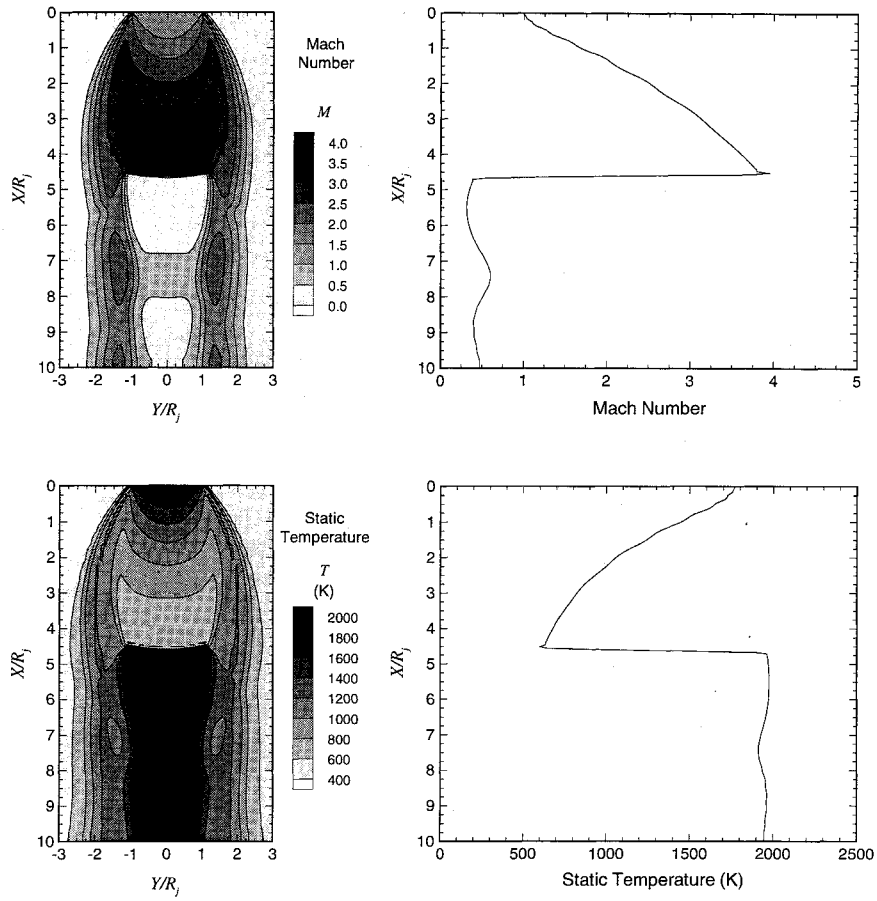

Fig. 6 Calculated contours and centerline distributions of Mach number and temperature in the reacting underexpanded jet, where P_0 = 160 kPa (1.58 atm), T_0 = 2000 K, P_b = 11 kPa (0.11 atm), and Φ = 1.0 (H_2-air).

line shape is resolved with only a total of 60 data points (i.e., one data point every 500 MHz-VIS tuned by the laser). Collecting fewer OH fluorescence data points considerably reduces the total acquisition time, since each OH fluorescence data point requires a minimum of 1 s to average over 10 laser pulses. Line-center locations are determined by scaling the frequency axis to match the 2-GHz-VIS interferometer fringe spacing, and fitting Gaussian and Voigt line shapes to the iodine and OH signals, respectively.

Results and Discussion

Figure 9 shows sample Doppler-shifted spectra from three points along the centerline of the reacting underexpanded jet core. At each point the results from a scan in each of the two counterpropagating directions is shown in addition to the simultaneously acquired iodine spectra that are used as an absolute frequency reference for the two directions. The increasing shift and narrowing line shape are evident as the velocity increases and the pressure and temperature decrease from the nozzle exit to the Mach disk. The noise in these spectral scans will be discussed later.

Figure 10 shows the results of the pointwise velocity measurements along the jet centerline, compared with the calculated velocity profile. Each data point represents an average of three frequency shifts measured from three separate scans for each of the two counterpropagating directions. The axial velocity at each point is given by

$$u = \frac{\lambda(\Delta\nu_1 - \Delta\nu_2)}{2\cos\theta} \tag{8}$$

where θ is the angle the laser beam makes with the jet axis (deg), and $\Delta\nu_1$ and $\Delta\nu_2$ are the measured average frequency shifts in the two directions (see Fig. 1). The vertical error bars in Fig. 10 represent the uncertainty 2σ for the average measured velocity at each location. The horizontal error bars represent the $\pm 0.075R_j$ uncertainty in the absolute position in the jet . (Note that the point-to-point spatial uncertainty was $\pm 0.003R_j$, owing to the use of a precision translation stage.) The velocities inside the measured supersonic jet core agree on average with the calculated values to within 1.3%, with the maximum difference being 2.9%. The Mach disk location was measured to be approximately $0.26R_j$ upstream of the calculated position, not an uncommon occurrence in underexpanded jet studies.[34-37]

The greater thickness of the measured Mach disk and the rounding of the velocity profile at the normal shock location result from unsteadiness in the shock position. The shock unsteadiness is caused by combustion-related disturbances that are generated upstream of the nozzle exit. These disturbances travel downstream and, upon traversing one of the shock waves, produce significant acoustic energy. The resulting sound waves travel back upstream through the subsonic flow outside the jet, and initiate instabilities in the boundary layer at the nozzle exit, thereby completing a resonant feedback loop. The noise created by these disturbances is characterized by high-amplitude, discrete tones (referred to as screech),[38] which cause fluctuations in the jet pressure ratio and, therefore, the Mach disk location.

In order to quantify the movement of the Mach disk, the pressure fluctuations in the combustion and vacuum chambers of the reacting underexpanded jet facility were measured with a high-speed pressure transducer (Kulite XCQ-093-50A). Typical traces of the pressure fluctuations in the combustion chamber and vacuum chamber are shown in Fig. 11. The low-frequency fluctuations in the combustion chamber are on the order of ± 1.2 kPa in magnitude and occur with a characteristic time of a few seconds, well within the minute required

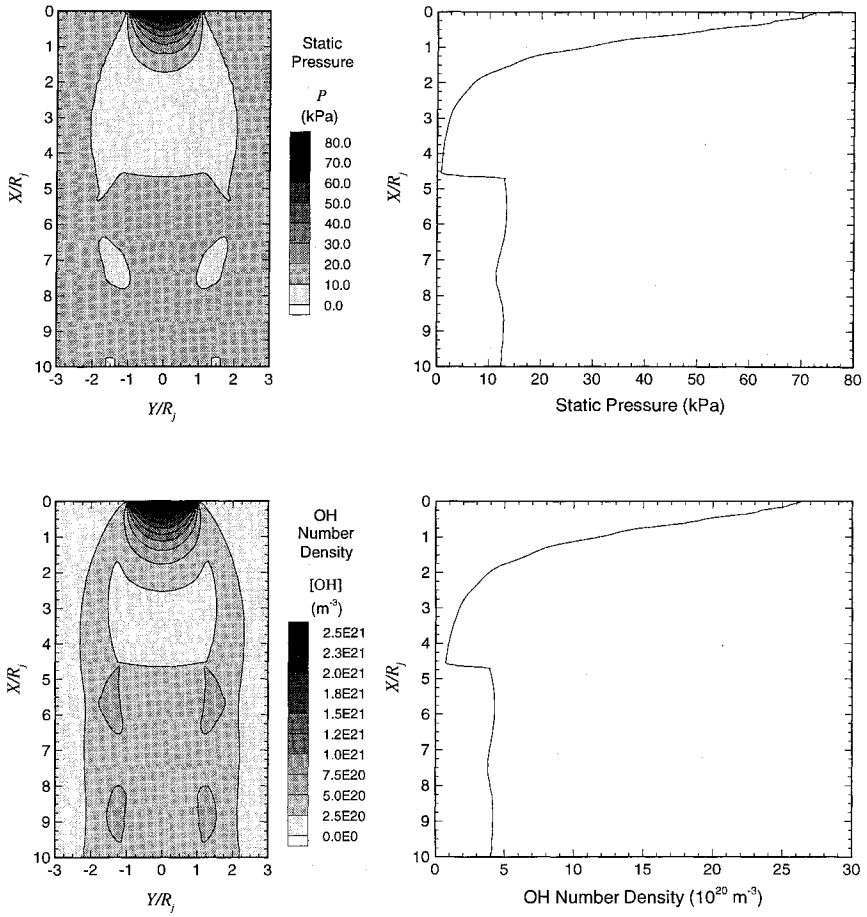

Fig. 7 Calculated contours and centerline distributions of pressure and OH number density in the reacting underexpanded jet, where P_0 = 160 kPa (1.58 atm), T_0 = 2000 K, P_b = 11 kPa (0.11 atm), and Φ = 1.0 (H_2-air).

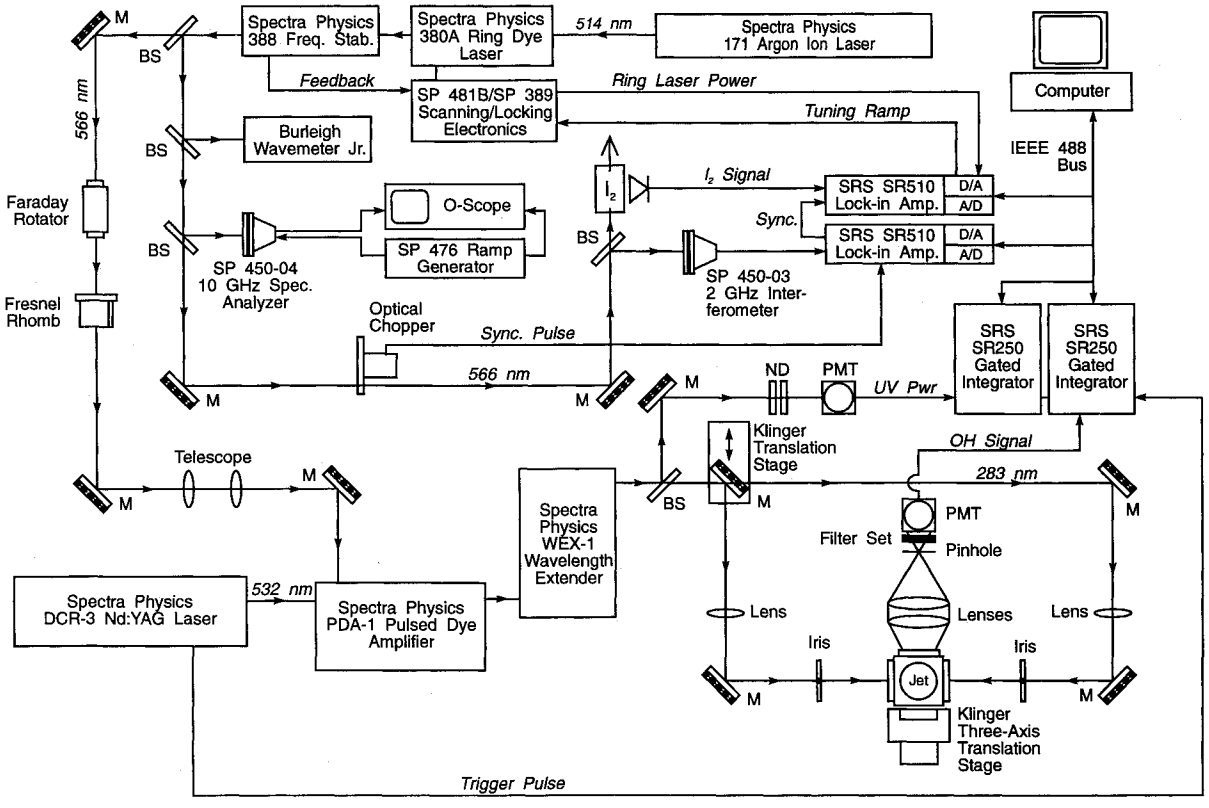

Fig. 8 Optical setup for the reacting underexpanded jet experiment including the pulse-amplified, narrow-linewidth, uv laser source for OH LIF velocity measurements.

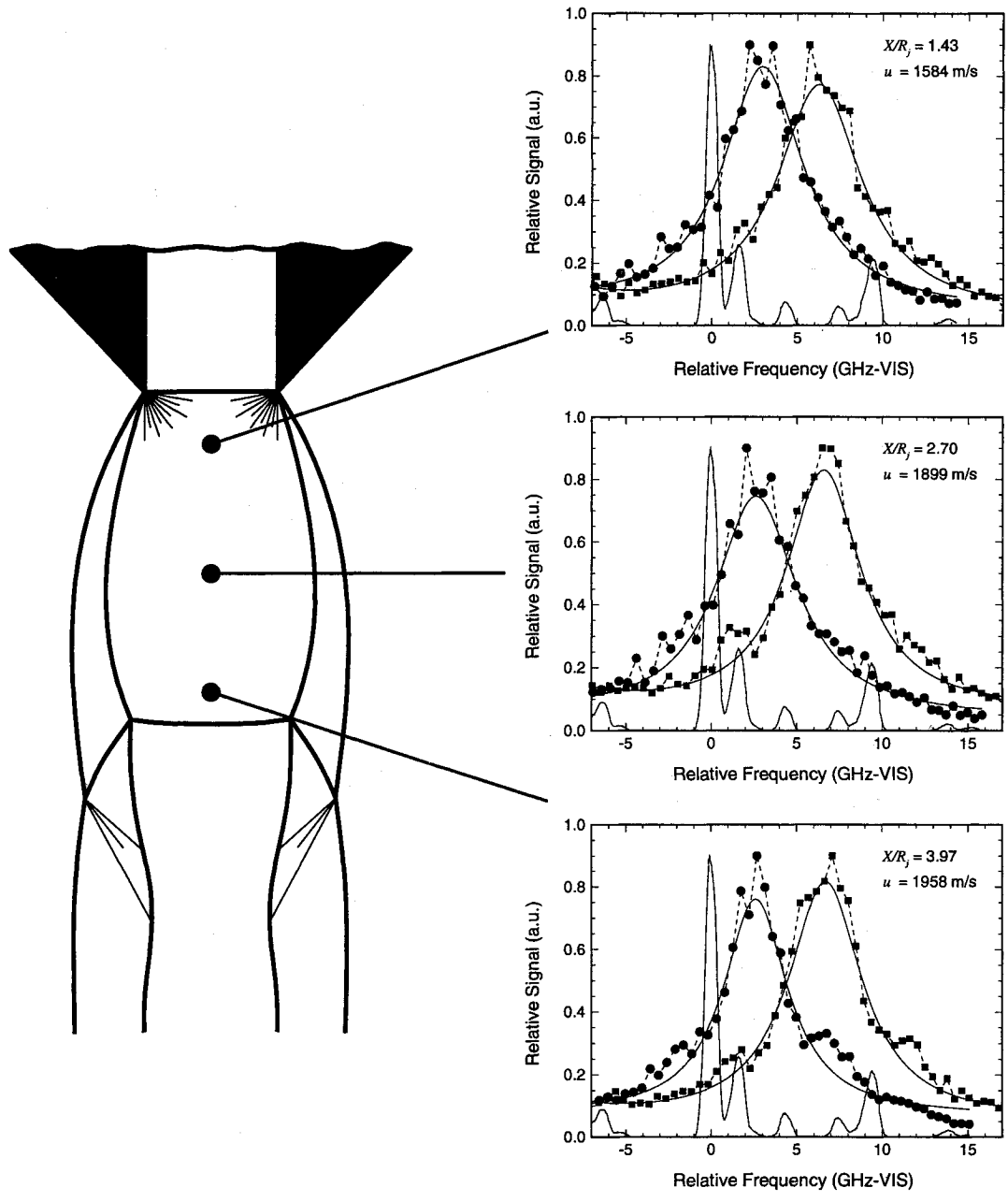

Fig. 9 Spectra at three points in the core of the reacting underexpanded jet for the two counterpropagating-beam directions. Also shown is the I_2 spectrum acquired for an absolute frequency reference.

for a complete scan of the OH absorption line. The fluctuations in the vacuum chamber were measured to be approximately ±1.0 kPa in magnitude at a frequency of ~38 kHz. The effect these fluctuations have on the Mach disk location X_M can be estimated by using the relationship for the normalized Mach disk location given in Ref. 35

$$X_M/R_j = 1.290\sqrt{P_0^{ex}/P_b} \tag{9}$$

where P_0^{ex} (i.e., the stagnation pressure at the nozzle exit after the Fanno line expansion through the nozzle tube) has been substituted for P_0. By differentiating Eq. (9), the fluctuation in the normalized Mach disk location is given by

$$\frac{\delta(X_M/R_j)}{X_M/R_j} = \frac{1}{2}\sqrt{\left|\frac{\delta P_0^{ex}}{P_0^{ex}}\right| + \left|\frac{\delta P_b}{P_b}\right|} \tag{10}$$

For the typical stoichiometric jet, where P_0^{ex} = 131.4 kPa and P_b = 11.1 kPa, the percent fluctuations for the combustion and vacuum chambers are ±0.9 and ±9.0%, respectively. The fluctuation in X_M/R_j is calculated to be ±5.0%, which is in good agreement with the apparent thickness of the measured Mach disk.

The reacceleration of the flow downstream of the Mach disk is expected as the throat-like condition is approached (see Fig. 1); however, the measured velocity reached a maximum of 1054 m/s, whereas the calculated reached only 542 m/s. This discrepancy in the region downstream of the Mach disk may be because the turbulent shear layers that create the throat-like condition are not well-predicted in the laminar calculation.

Laser-induced fluorescence measurements are often limited in their accuracy by the "shot" noise associated with the number of signal photons collected. In order to determine if the velocity measurement in the reacting underexpanded jet was shot-noise limited, or whether other dominant sources were present, the experimental SNR was compared to the theoretical shot-noise-limited value. The theoretical SNR was calculated using Eqs. (3–7), the parameters listed in Table A1

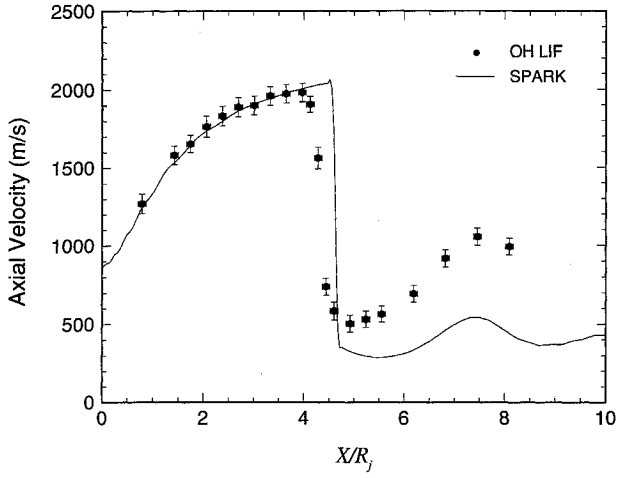

Fig. 10 Pointwise measurements of velocity along the centerline of the reacting underexpanded jet compared to the results from the axisymmetric Navier-Stokes calculation. The vertical error bars represent the uncertainties 2σ for the average measured velocities. The horizontal error bars represent the absolute position error in the jet.

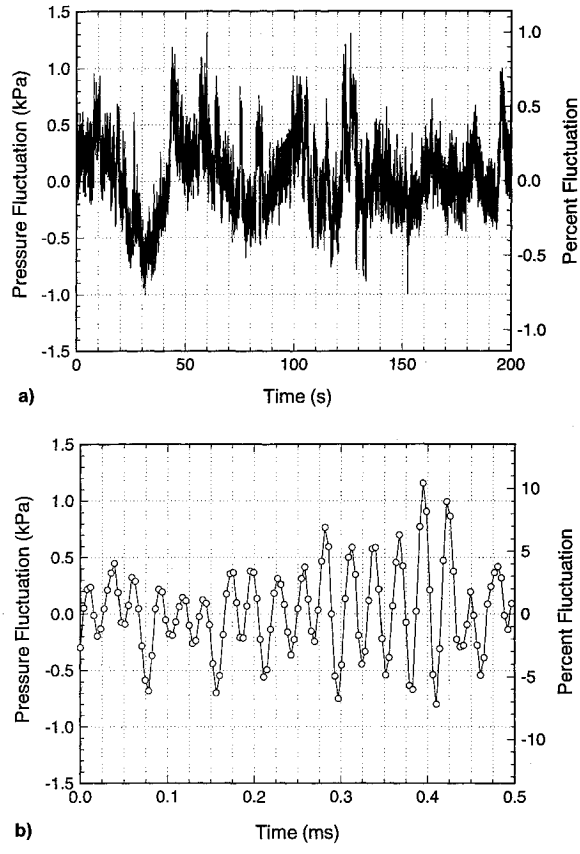

Fig. 11 Typical pressure traces for a) the combustion chamber and b) the vacuum chamber of the reacting underexpanded jet facility.

(located in the Appendix), the flow conditions calculated with the SPARK code, and the shot-noise-limited-detecton relationship, $\mathrm{SNR}_{\mathrm{calc}} = \sqrt{N_{\mathrm{LP}} S_F^{\mathrm{tot}}}$,[39] where N_{LP} is the number of laser pulses averaged. For the experimental signal-to-noise, $\mathrm{SNR}_{\mathrm{exp}} \cong \sqrt{PTS/\chi^2}$ is used, where PTS is the number of data points making up the Voigt profile, and χ^2 represents the "goodness of fit" of a Voigt line shape to the experimental data.[40] Thus, $\mathrm{SNR}_{\mathrm{exp}}$ represents the inverse of the rms noise along the Voigt curve. The calculated and experimental SNR values of the velocity measurements in the reacting underexpanded jet flowfield are shown in Fig. 12. The consistently low experimental SNR clearly indicates that the experimental signal was not shot-noise limited. The extra noise may be

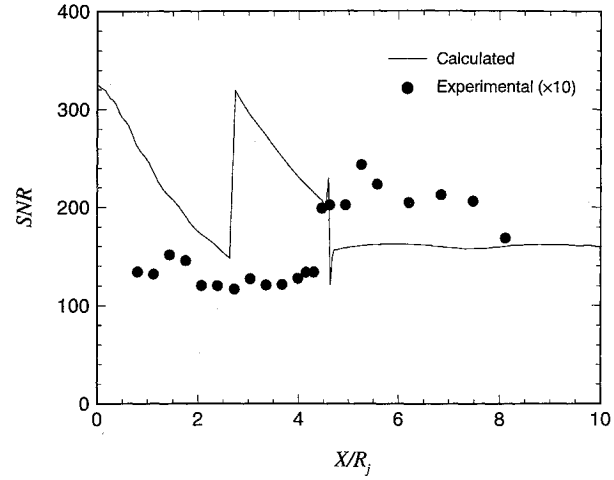

Fig. 12 Calculated and experimental (× 10) signal-to-noise ratio for the underexpanded jet experiment. The calculation includes the use of a 0.7-ND filter for $0 < X/R_j < 2.71$ and $X/R_j > 4.62$.

caused by the same combustion-related instabilities in the combustion chamber of the jet that were discussed earlier in relation to the Mach disk instability. Combustion instabilities, perhaps caused by incomplete and unsteady fuel-air mixing, would also cause total temperature fluctuations leading to velocity and OH concentration fluctuations in the underexpanded jet. Such fluctuations would add noise to the spectral scans (as seen in Fig. 9), increasing the χ^2 of the spectral Voigt fits and lowering the experimental SNR.

A Monte Carlo simulation was performed to determine the relationship between the uncertainty in the measured total shifts (i.e., the uncertainty in the curve fit parameters $\Delta\nu_1$ and $\Delta\nu_2$), and the Voigt line shape, the number of data points, and the signal-to-noise ratio. Random noise of varying magnitude was added to Voigt curves of varying widths and varying number of points. A Voigt function was fit to the noisy curves, and the difference between the fit centerline locations and the original centerline location was recorded for later statistical analysis over 100 trials. The uncertainty 2σ in the measured total shift GHz-uv was found to be related to the signal-to-noise ratio, the number of data points, and the Voigt line shape by[30]

$$\delta\Delta\nu_{1,2}^{\mathrm{fit}} = \left\{ \frac{16.632}{\mathrm{SNR}} \left(\frac{\Delta\nu_V}{PTS} \right)^{0.5} \left[\frac{\partial V(D, B')/\partial\nu}{V(D, B')} \right]^{-0.702} \right\}_{1,2} \tag{11}$$

where the term in the square brackets is the normalized slope of the Voigt line shape at the half-maximum point, where $(\nu - \nu_0)/\Delta\nu_V = 0.5$. With the Voigt line shapes and signal-to-noise levels measured here, the uncertainty in the total measured shifts from the curve fits $\delta\Delta\nu_{1,2}^{\mathrm{fit}}$ is on average ± 0.270 GHz-uv in the jet core. There is an additional contribution to the random uncertainty that arises through the power normalization procedure. With the incident irradiance levels used here, where $I = 5.2(10)^{11}$ W/m^2, the OH absorption transition is saturated to various degrees, depending on the local thermodynamic conditions at the measurement point. Since these conditions are not known, the relationship between the fluorescence signal and the incident irradiance is also not known. This additional uncertainty due to the power normalization procedure $\delta\Delta\nu_{1,2}^{pwr}$ was estimated (for the average measured rms laser power fluctuations of $\pm 4.9\%$) by comparing curve fits with (assuming $S_F^{\mathrm{tot}} \propto I$) and without power normalization and was determined to be on average ± 0.154 GHz-uv in the jet core. By taking the square root of the sum of the squares of the two random uncertainties described above, the total random uncertainty $\delta\Delta\nu_{1,2}^{\mathrm{tot}}$ is ± 0.310 GHz-uv. The systematic uncertainty due to the uncertainty in the measurement of the

beam angle $\delta\theta$ is ± 0.25 deg. The fractional uncertainty in the velocity, calculated using Eq. (8), is given by[40]

$$\frac{\delta u}{u} = \sqrt{2\left(\frac{1}{\Delta\nu_1 - \Delta\nu_2}\right)^2 (\delta\Delta\nu_{1,2}^{\text{tot}})^2 + \left(\frac{\sin\theta}{\cos\theta}\right)^2 \left(\frac{\pi}{180}\,\delta\theta\right)^2} \tag{12}$$

and upon substitution of the beam angle ($\theta = 54$ deg), the average Doppler shift $\Delta\nu_1 - \Delta\nu_2 = 7.312$ GHz-uv, and the random $\delta\Delta\nu_{1,2}^{\text{tot}}$ and systematic $\delta\theta$ uncertainties described above, the fractional uncertainty 2σ for a velocity measurement in the jet core is on average $\pm 6.0\%$. By averaging three measurements, the fractional uncertainty in the average velocity reduces to a calculated value of $\pm 3.5\%$. This is consistent with the maximum measured difference of 2.9% in the supersonic jet core.

Many sources of systematic error are eliminated by the counterpropagating-beam technique. By using counterpropagating beams, errors due to effects that are of the same magnitude and sense for each beam direction automatically cancel. These types of effects include saturation of the transition, trapping of the fluorescence signal, or detection of fluorescence from adjacent resonance lines. One potential source of error that is not canceled by the counterpropagating-beam technique is that caused by laser beam absorption. The absorption of the laser beam at each location in the flow is a function of the local velocity and thermodynamic conditions. Since the net incident irradiance at each measurement location is a function of the integrated absorption along the beam path, it may be nonuniform in laser frequency, depending on the velocities and thermodynamic conditions of the regions of the flow through which the beam has traversed. With the counterpropagating-beam approach, the flow regions through which the beam passes to reach a particular point will be different for the two beam directions. The signal from each direction could be unequally affected, thereby increasing the errors in determining the line center frequencies. This effect could be significant in situations where there are regions of high OH concentration, where long beam paths are required, and/or where $I \ll I_{\text{sat}}$. For the measurements presented herein, where $I/I_{\text{sat}} > 1000$, $N_{\text{OH}} < 6.5(10)^{20}$ m^{-3}, and the beam path is less than 5 mm, no absorption effects were expected or detected. If laser beam absorption proves to be a source of systematic error, it can be reduced by using a satellite line, such as the (1,0) $Q_{21}(5)$ located ~34 GHz-uv to the lower frequency side of the (1,0) $Q_1(5)$ main line. Typically, such satellite lines have absorption coefficients that are an order of magnitude less than those of the main lines. Since absorption problems occur in flows with relatively large absorber densities, the favorable absorber population will partially compensate for the weaker fluorescence signal due to the smaller absorption coefficient of the satellite line.

Summary and Conclusions

A high-resolution OH LIF velocity measurement technique was developed for use in steady, high-speed, reacting flows. A narrow-linewidth laser source was tuned through an isolated OH absorption line to measure the Doppler-shifted line center frequency relative to an iodine reference line. A counterpropagating-beam approach was used to eliminate the collisional impact shift and minimize systematic errors. Pointwise measurements of velocity were made in a unique reacting underexpanded jet facility as a test of the technique over a wide range of flow conditions. The measured and calculated velocities in the supersonic jet core agree on average to within 1.3%. The uncertainty in the velocity measurement in the jet core was on average $\pm 6.0\%$ for a single measurement and $\pm 3.5\%$ for the average value of three scans. Potential errors caused by absorption effects were not detected in these measurements.

Future work includes conducting planar velocity measurements in the reacting underexpanded jet using an extension of the pointwise technique reported herein and applying the technique in a model scramjet combustor. Results from the combustor experiment will provide much needed data for the validation of CFD codes to be used for scramjet combustor design and development.

Appendix: Calculation of the Total Fluorescence Signal

The fundamental relations for calculating the total fluorescence signal are given by Eqs. (3–7). The details of the evaluation of the terms in these equations are given in this Appendix. The total Einstein coefficients for spontaneous emission are calculated using[30]

$$A_{\nu'} = \sum_{\nu''} \left(\sum_{N'} \sum_{N''} f_{N'} A_{N'N''} \right)_{\nu'\nu''} \tag{A1}$$

where $f_{N'}$ is the population fraction of the excited state rotational level N' [i.e., the number of molecules in rovibrational level (N', ν') divided by the total number of molecules in vibrational level ν'], and $A_{N'N''}$ is the Einstein coefficient for spontaneous emission from the excited state rotational level N' to the ground state rotational level N''. The effective photon emission rates are defined as[30]

$$A_{\nu'\nu''}^{\text{eff}} = \left[\sum_{N'} \sum_{N''} F(\lambda_{N'N''}) f_{N'} A_{N'N''} \right]_{\nu'\nu''} \tag{A2}$$

where $F(\lambda_{N'N''})$ is the filter transmissivity at the transition-dependent wavelength $\lambda_{N'N''}$.

The steady-state population of the directly pumped energy level can be related to the total OH number density by[30]

$$N_{\text{ss}} = \sqrt{\frac{4(\ln 2)}{\pi}} \frac{B_{10}\tau_1}{c\Delta\nu_D} \frac{I}{\sqrt{1 + I/I_{\text{sat}}}} V(D, B') f_{N''} N_{\text{OH}} \tag{A3}$$

where B_{10} is the Einstein coefficient for stimulated absorption from the $\nu'' = 0$ ground state to the $\nu' = 1$ excited state (m^3/J·s^2), c is the speed of light (m/s), I is the laser irradiance (W/m^2), $\Delta\nu_D$ is the Doppler linewidth (s^{-1}), $f_{N''}$ is the ground state Boltzmann population fraction (i.e., the number of molecules in rovibrational level N'', ν'' divided by the total number of molecules in the ground state electronic level), N_{OH} is the total OH number density (m^{-3}), I_{sat} is the saturation irradiance (W/m^2), and $V(D, B')$ is the Voigt line shape integral. The saturation irradiance is defined as[30]

$$I_{\text{sat}} = \frac{c\pi\Delta\nu_C\tau_1}{2B_{10}\left[f_{N''}\left(\frac{\tau_0 + V}{\tau_0}\right) + f_{N'}\left(\frac{g_{N''}}{g_{N'}}\right)\right]} \tag{A4}$$

where $\Delta\nu_C$ is the collisional linewidth (s^{-1}), $f_{N'}$ is the population fraction of the directly pumped excited state, and $g_{N''}$ and $g_{N'}$ are the energy level degeneracies of the ground and directly pumped excited states, respectively. The Voigt integral represents the convolution of the two predominant broadening mechanisms, collisional and Doppler, and is expressed as

$$V(D, B') = \frac{B'}{\pi} \int_{-\infty}^{+\infty} \frac{\exp(-y^2)}{(B')^2 + (D - y)^2}\,dy \tag{A5}$$

Table A1 Experimental parameters and coefficients used for calculating an estimate of the photon yield for pointwise OH LIF velocity measurements in the reacting underexpanded jet

OH (1,0) Q_1 (5) Absorption line
$\nu_0 = 1.061(10)^{15}$ Hz (Ref. 29)
$B_{01} = 2.859(10)^{17}$ m³/J·s² (Ref. 28)
$A_{N'N''}$ (Ref. 28)
$\lambda_{N'N''}$ (Ref. 29)
Signal detection
$\eta = 0.17$[a]
$\Omega = 0.226$
$V_C = 2.7(10)^{-12}$ m³
$\Delta t_G = 4.0(10)^{-8}$ s
$N_{LP} = 10$
Laser beam
$E_L = 0.12(10)^{-3}$ J[b]
$A_L = 1.77(10)^{-8}$ m²
$\Delta t_L = 1.3(10)^{-8}$ s
$I = 5.2(10)^{11}$ W/m²
Collisional quenching coefficients[c]
$\sigma_{N_2} = 0.15 + 0.58 \exp(-T/1000) + 3.50 \exp(-T/500)$ m²
$\sigma_{H_2O} = 2.56 + 55.70 \exp(-T/1000) + 42.00 \exp(-T/500)$ m²
$\sigma_{H_2} = 0.18 + 8.16 \exp(-T/1000) + 2.87 \exp(-T/500)$ m²
$\sigma_{O_2} = 0.60 + 15.70 \exp(-T/1000) + 5.03 \exp(-T/500)$ m²
Collisional broadening coefficients[d]
$\gamma_{N_2} = 7.54(10)^8[T]^{-0.54}$ s⁻¹/kPa (Ref. 45)
$\gamma_{H_2O} = 6.35(10)^9[T]^{-0.66}$ s⁻¹/kPa (Ref. 46)
$\gamma_{H_2} = 9.27(10)^8[T]^{-0.5}$ s⁻¹/kPa (Ref. 47)
$\gamma_{O_2} = 7.26(10)^8[T]^{-0.5}$ s⁻¹/kPa (Ref. 47)
Vibrational transfer coefficient[e]
$V = [0.74 - (0.029 \times N')] \times Q$

[a]Includes estimate of reflection losses through jet window and collection optics, and the 0.7-ND filter for $0 < X/R_j < 2.71$ and $X/R_j > 4.62$.
[b]Estimate of remaining energy after reflecting from mirrors and passing through focusing optics and jet window.
[c]Fit to data in Ref. 48 using equations of the form suggested in Ref. 44. Only values for N_2 and H_2O are required for stoichiometric mixtures with complete combustion.
[d]Inferred values for γ_i from the specified references assuming a $T^{-0.5}$ dependence (except as noted for H_2O and N_2) given by a hard sphere (constant cross section) collision model.[49] Only values for N_2 and H_2O are required for stoichiometric mixtures with complete combustion.
[e]Linear fit to the data in Ref. 50.

where

$$y = \sqrt{4(\ln 2)}[(\nu - \nu_0)/\Delta\nu_D] \quad \text{(A6)}$$

$$D = \sqrt{4(\ln 2)}[(\nu_L - \nu_0)/\Delta\nu_D] \quad \text{(A7)}$$

$$B' = \sqrt{\ln 2}(\Delta\nu_H/\Delta\nu_D) \quad \text{(A8)}$$

with the laser frequency ν_L, molecular transition frequency ν_0, and homogeneous linewidth $\Delta\nu_H = \Delta\nu_C\sqrt{1 + I/I_{sat}}$. The Voigt linewidth is given to a good approximation by[41]

$$\Delta\nu_V = (\Delta\nu_H/2) + \sqrt{(\Delta\nu_H^2/4) + \Delta\nu_D^2} \quad \text{(A9)}$$

For OH, the Doppler width (s^{-1}) can be calculated using

$$\Delta\nu_D = 1.737(10)^{-7}\nu_0\sqrt{T} \quad \text{(A10)}$$

where T is the static temperature (K), and the collisional width (s^{-1}) can be calculated using

$$\Delta\nu_C = \sum_i \gamma_i p_i \quad \text{(A11)}$$

where γ_i (s^{-1}/kPa) is the temperature-dependent broadening parameter, and p_i (kPa) is the partial pressure of species i.

A few assumptions were made regarding the rotational transfer in the excited states to simplify the above model. For example, studies of vibrational energy transfer in $A^2\Sigma^+$ OH at room temperature[42] and in flames[43] have shown that, although some rotational relaxation does occur in $\nu' = 1$ before vibrational transfer to $\nu' = 0$, the molecules redistribute themselves mostly to the rotational levels immediately adjacent to the directly pumped level. Therefore, the rotational distribution in $\nu' = 1$ is assumed frozen in the directly pumped rotational level (i.e., $f_{N'} = 1$), and the values used for V and $A_{N'N''}$ are those ascribed to that level. It was also found[42,43] that the rotational distribution in the $\nu' = 0$ level, after vibrational transfer from the $\nu' = 1$ level, is approximately thermal. It is, therefore, reasonable to assume that the rotational population in the $\nu' = 0$ level is distributed in a Boltzmann fashion with a temperature equal to the translational temperature of the gas. In addition, the quenching rates for $\nu' = 1$ and $\nu' = 0$ are assumed to be equal and are calculated using

$$Q = \sum_i n_i\nu_i\sigma_i \quad \text{(A12)}$$

where n_i is the number density (m^{-3}), ν_i is the relative collision velocity (m/s), and σ_i is the quenching cross section (m^2) of specie i. The temperature- and rotational-level-dependent quenching cross sections are determined using the method outlined in Ref. 44. Table A1 includes a summary of the experimental parameters, collisional quenching coefficients, collisional broadening coefficients, and vibrational transfer coefficient used for calculating the photon yield in the underexpanded jet experiment.

Acknowledgments

This research was supported by NASA Grant NAG-1-795 from the NASA Langley Research Center (LaRC), G. B. Northam, technical monitor. Special thanks are given to R. J. Exton (LaRC) for providing the laser frequency stabilizer, to J. P. Drummond (LaRC) for providing the axisymmetric version of SPARK, and to J. M. Donohue (UVa) for assisting with the jet calculation.

References

[1]McKenzie, R. L., "Progress in Laser-Spectroscopic Techniques for Aerodynamic Measurements: An Overview," *AIAA Journal*, Vol. 31, No. 3, 1993, pp. 465–477.

[2]Maurice, M. S., "The Effect of Particle Dynamics on Laser Velocimetry Measurement Bias in Compressible Vortical Flows," AIAA Paper 91-0292, Jan. 1991.

[3]Maurice, M. S., "A Method to Quantify and Correct Particle Velocity Bias in Laser Velocimetry Measurements," AIAA Paper 92-0764, Jan. 1992.

[4]Miles, R. B., Connors, J., Markowitz, E., Howard, P., and Roth, G., "Instantaneous Supersonic Velocity Profiles in an Underexpanded Sonic Air Jet by Oxygen Flow Tagging," *Physics of Fluids A*, Vol. 1, No. 2, 1989, pp. 389–393.

[5]Boedeker, L. R., "Velocity Measurement by H_2O Photolysis and Laser-Induced Fluorescence of OH," *Optics Letters*, Vol. 14, No. 10, 1989, pp. 473–475.

[6]Miles, R., and Lempert, W., "Two-Dimensional Measurement of Density, Velocity, and Temperature in Turbulent High-Speed Air Flows by UV Rayleigh Scattering," *Applied Physics B*, Vol. 51, No. 1, 1990, pp. 1–7.

[7]She, C. Y., "Proposal for the Measuring Molecular Velocity Vector with Single-Pulse Coherent Raman Spectroscopy," *Applied Physics B*, Vol. 32, No. 1, 1983, pp. 49–52.

[8]Gustafson, E. K., McDaniel, J. C., and Byer, R. L., "CARS Measurement of Velocity in a Supersonic Jet," *IEEE Journal of Quantum Electronics*, Vol. QE-17, No. 12, 1981, pp. 2258, 2259.

[9]Herring, G. C., Fairbank, W. M., Jr., and She, C. Y., "Observation and Measurement of Molecular Flow Using Stimulated Raman Gain Spectroscopy," *IEEE Journal of Quantum Electronics*, Vol. QE-17, No. 10, 1981, pp. 1975, 1976.

[10]Moosmüller, H., Herring, G. C., and She, C. Y., "Two-Component Velocity Measurements in a Supersonic Nitrogen Jet with Spatially Resolved Inverse Raman Spectroscopy," *Optics Letters*, Vol. 9, No. 12, 1984, pp. 534–538.

[11]Exton, R. J., and Hillard, M. E., "Raman Doppler Velocimetry: A Unified Approach for Measuring Molecular Flow Velocity, Temperature, and Pressure," *Applied Optics*, Vol. 25, No. 1, 1986, pp.

14–21.

[12]Herring, G. C., Moosmüller, H., Lee, S. A., and She, C. Y., "Flow Velocity Measurements with Stimulated Rayleigh-Brillouin-Gain Spectroscopy," *Optics Letters*, Vol. 8, No. 12, 1983, pp. 602–604.

[13]Fletcher, D. G., and McDaniel, J. C., "Laser-Induced Iodine Fluorescence Technique for Quantitative Measurement in a Non-reacting Supersonic Combustor," *AIAA Journal*, Vol. 27, No. 5, 1989, pp. 575–580.

[14]Westblom, U., and Aldén, M., "Spatially Resolved Flow Velocity Measurements Using Laser-Induced Fluorescence from a Pulsed Laser," *Optics Letters*, Vol. 14, No. 1, 1989, pp. 9–11.

[15]McDaniel, J. C., Hiller, B., and Hanson, R. K., "Simultaneous Multiple-Point Velocity Measurements Using Laser-Induced Iodine Fluorescence," *Optics Letters*, Vol. 8, No. 1, 1983, pp. 51–53.

[16]Hartfield, R. J., Hollo, S. D., and McDaniel, J. C., "Planar Measurement Technique for Compressible Flows Using Laser-Induced Iodine Fluorescence," *AIAA Journal*, Vol. 31, No. 3, 1993, pp. 483–490.

[17]Cheng, S., Zimmermann, M., and Miles, R. B., "Supersonic-Nitrogen Flow-Field Measurements with the Resonant Doppler Velocimeter," *Applied Physics Letters*, Vol. 43, No. 2, 1983, pp. 143–145.

[18]Zimmermann, M., and Miles, R. B., "Hypersonic-Helium-Flow-Field Measurements with the Resonant Doppler Velocimeter," *Applied Physics Letters*, Vol. 37, No. 10, 1980, pp. 885–887.

[19]Paul, P. H., Lee, M. P., and Hanson, R. K., "Molecular Velocity Imaging of Supersonic Flows Using Pulsed Planar Laser-Induced Fluorescence of NO," *Optics Letters*, Vol. 14, No. 9, 1989, pp. 417–419.

[20]DiRosa, M. D., Chang, A. Y., and Hanson, R. K., "CW Dye Laser Technique for Simultaneous, Spatially-Resolved Measurements of Temperature, Pressure, and Velocity of NO in an Underexpanded Free Jet," AIAA Paper 92-0006, Jan. 1992.

[21]Marinelli, W. J., Kessler, W. J., Allen, M. G., Davis, S. J., and Arepalli, S., "Copper Atom Based Measurements of Velocity and Turbulence in Arc Jet Flows," AIAA Paper 91-0358, Jan. 1991.

[22]Erwin, D. A., Pham-Van-Diep, G. C., and Deininger, W. D., "Laser-Induced Fluorescence Measurements of Flow Velocity in High-Power Arcjet Thruster Plumes," *AIAA Journal*, Vol. 29, No. 8, 1991, pp. 1298–1303.

[23]Liebeskind, J. G., Hanson, R. K., and Cappelli, M. A., "Laser-Induced Fluorescence of Atomic Hydrogen in an Arcjet Thruster," AIAA Paper 92-0678, Jan. 1992.

[24]Chang, A. Y., Battles, B. E., and Hanson, R. K., "Simultaneous Measurements of Velocity, Temperature, and Pressure Using Rapid CW Wavelength-Modulation Laser-Induced Fluorescence of OH," *Optics Letters*, Vol. 15, No. 12, 1990, pp. 706–708.

[25]Paul, P. H., and Hanson, R. K., "Applications of Planar Laser-Induced Fluorescence Imaging Diagnostics to Reacting Flows," AIAA Paper 90-1848, July 1990.

[26]Traving, G., "Interpretation of Line Broadening and Line Shift," *Plasma Diagnostics*, edited by W. Lochte-Holtgreven, North-Holland, Amsterdam, 1968, pp. 66–134.

[27]McDaniel, J. C., "Laser Methods for Nonintrusive Measurement of Supersonic, Hydrogen-Air Combustion Flowfields," *Optical Methods in Flow and Particle Diagnostics: ICALEO 1988 Proceedings*, Vol. 67, 1988, pp. 209–218.

[28]Dimpfl, W. L., and Kinsey, J. L., "Radiative Lifetimes of OH($A^2\Sigma$) and Einstein Coefficients for the A-X System of OH and OD," *Journal of Quantitative Spectroscopy and Radiative Transfer*, Vol. 21, No. 3, 1979, pp. 233–241.

[29]Diecke, G. H., and Crosswhite, H. M., "The Ultraviolet Bands of OH: Fundamental Data," *Journal of Quantitative Spectroscopy and Radiative Transfer*, Vol. 2, No. 2, 1962, pp. 97–199.

[30]Klavuhn, K. G., "Spatially-Resolved Velocity Measurements in Steady, High-Speed, Reacting Flows Using Laser-Induced OH Fluorescence," Ph.D. Dissertation, Dept. of Mechanical, Aerospace, and Nuclear Engineering, Univ. of Virginia, Charlottesville, VA, 1994.

[31]Klavuhn, K. G., and McDaniel, J. C., "Reacting Underexpanded Jet for Spectroscopic Applications," *Review of Scientific Instruments* (to be published).

[32]Drummond, J. P., "A Two-Dimensional Numerical Simulation of a Supersonic, Chemically Reacting Mixing Layer," NASA TM 4055, 1988.

[33]Reynolds, W. C., "The Element Potential Method for Chemical Equilibrium Analysis: Implementation in the Interactive Program STANJAN—Version 3," Dept. of Mechanical Engineering, Stanford Univ., Stanford, CA, 1986.

[34]Adamson, T. C., Jr., and Nicholls, J. A., "On the Structure of Jets from Highly Underexpanded Nozzles into Still Air," *Journal of the Aerospace Sciences*, Vol. 26, No. 1, 1959, pp. 16–24.

[35]Crist, S., Sherman, P. M., and Glass, D. R., "Study of the Highly Underexpanded Sonic Jet," *AIAA Journal*, Vol. 4, No. 1, 1966, pp. 68–71.

[36]Werle, M. J., Shaffer, D. G., and Driftmyer, R. T., "Freejet Terminal Shocks," *AIAA Journal*, Vol. 8, No. 12, 1970, pp. 2295–2297.

[37]Davidor, W., and Penner, S. S., "Shock Standoff Distances and Mach-Disk Diameters in Underexpanded Sonic Jets," *AIAA Journal*, Vol. 9, No. 8, 1971, pp. 1651–1653.

[38]Powell, A., "The Noise Emanating from a Two-Dimensional Jet Above the Critical Pressure," *Aeronautical Quarterly*, Vol. 4, 1953, pp. 103–122.

[39]Eckbreth, A. C., *Laser Diagnostics for Combustion Temperature and Species*, Abacus Press, Cambridge, MA, 1988.

[40]Holman, J. P., *Experimental Methods for Engineers*, McGraw-Hill, New York, 1989.

[41]Posener, D. W., "The Shape of Spectral Lines: Tables of the Voigt Profile," *Australian Journal of Physics*, Vol. 12, No. 2, 1959, pp. 184–196.

[42]Lengel, R. K., and Crosley, D. R., "Energy Transfer in $A^2\Sigma^+$ OH: II. Vibrational," *Journal of Chemical Physics*, Vol. 68, No. 12, 1978, pp. 5309–5324.

[43]Smith, G. P., and Crosley, D. R., "Vibrational Energy Transfer in $A^2\Sigma^+$ OH in Flames," *Applied Optics*, Vol. 22, No. 10, 1983, pp. 1428–1430.

[44]Barlow, R. S., Dibble, R. W., and Lucht, R. P., "Simultaneous Measurement of Raman Scattering and Laser-Induced OH Fluorescence in Nonpremixed Turbulent Jet Flames," *Optics Letters*, Vol. 14, No. 5, 1989, pp. 263–265.

[45]Rea, E. C., Jr., Chang, A. Y., and Hanson, R. K., "Shock-Tube Study of Pressure Broadening of the $A^2\Sigma^+$-$X^2\Pi$ (0,0) Band of OH by Ar and N_2," *Journal of Quantitative Spectroscopy and Radiative Transfer*, Vol. 37, No. 2, 1987, pp. 117–127.

[46]Rea, E. C., Jr., Chang, A. Y., and Hanson, R. K., "Collisional Broadening of the $A^2\Sigma^+$-$X^2\Pi$ (0,0) Band of OH by H_2O and CO_2 in Atmospheric-Pressure Flames," *Journal of Quantitative Spectroscopy and Radiative Transfer*, Vol. 41, No. 1, 1989, pp. 29–42.

[47]Engleman, R., Jr., "Collisional Broadening of Transient Absorption Spectra: I. Hydroxyl Linewidths in the (0,0) (A→X) Transition at Low Temperatures," *Journal of Quantitative Spectroscopy and Radiative Transfer*, Vol. 9, No. 3, 1969, pp. 391–400.

[48]Garland, N. L., and Crosley, D. R., "On the Collisional Quenching of Electronically Excited OH, NH and CH in Flames," *Proceedings of the 21st Symposium (International) on Combustion*, The Combustion Inst., Pittsburgh, PA, 1986, pp. 1693–1702.

[49]Margenau, H., and Watson, W. W., "Pressure Effects on Spectral Lines," *Reviews of Modern Physics*, Vol. 8, No. 1, 1936, pp. 22–53.

[50]Crosley, D. R., "Collisional Effects on Laser-Induced Fluorescence Flame Measurements," *Optical Engineering*, Vol. 20, No. 4, 1981, pp. 511–521.